

Masses of the Main Asteroid Belt and the Kuiper Belt from the Motions of Planets and Spacecraft

E. V. Pitjeva · N. P. Pitjev

Received: 13 April 2017 / Accepted: 08 May 2018

Abstract – Dynamical mass estimates for the main asteroid belt and the trans-Neptunian Kuiper belt have been found from their gravitational influence on the motion of planets. Discrete rotating models consisting of moving material points have been used to model the total attraction from small or as yet undetected bodies of the belts. The masses of the model belts have been included in the set of parameters being refined and determined and have been obtained by processing more than 800 thousand modern positional observations of planets and spacecraft. We have processed the observations and determined the parameters based on the new EPM2017 version of the IAA RAS planetary ephemerides. The large observed radial extent of the belts (more than 1.2 au for the main belt and more than 8 au for the Kuiper belt) and the concentration of bodies in the Kuiper belt at a distance of about 44 au found from observations have been taken into account in the discrete models. We have also used individual mass estimates for large bodies of the belts as well as for objects that spacecraft have approached and for bodies with satellites. Our mass estimate for the main asteroid belt is $(4.008 \pm 0.029) \cdot 10^{-4} m_{\oplus}$ (3σ). The bulk of the Kuiper belt objects are in the ring zone from 39.4 to 47.8 AU. The estimate of its total mass together with the mass of the 31 largest trans-Neptunian Kuiper belt objects is $(1.97 \pm 0.030) \cdot 10^{-2} m_{\oplus}$ (3σ), which exceeds the mass of the main asteroid belt almost by a factor of 50. The mass

E. Pitjeva

Institute of Applied Astronomy of Russian Academy of Sciences, Kutuzov Quay 10, 191187
St.Petersburg, Russia
E-mail: evp@iaaras.ru

N. Pitjev

St.Petersburg State University, Universitetski pr. 28, Petrodvoretz, 198504, Russia; Institute of Applied Astronomy of Russian Academy of Sciences, Kutuzov Quay 10, 191187
St.Petersburg, Russia;
E-mail: ai@astro.spbu.ru

of the 31 largest trans-Neptunian objects (TNOs) is only about 40% of the total one.

Keywords :

Solar system, main asteroid belt, trans-Neptunian objects, Kuiper belt, planetary ephemerides.

Introduction

The Solar system has a complex structure that includes large bodies and a lot of small bodies moving under the action of mutual attraction. Since the accuracy of modern radio observations is a few meters, allowance for the gravitational influence of even comparatively small objects is required to properly represent the motion of bodies in the Solar system.

The attention of Solar system researchers to the main asteroid belt and the Kuiper belt has steadily increased in the last decades. Most of the asteroids that dangerously approach the Earth are associated with the main belt, and the prediction of their appearance, their sizes and number enters into the general important task to prevent dangerous collisions with the Earth. The interest in the distant Kuiper belt is maintained with the discovery of new trans-Neptunian objects (TNOs) and a refinement of their distribution in distances and sizes. This belt shows a varied structure of orbits, raising questions about its formation, the composition of the primordial material, and the early history of the Solar system.

The system of differential equations of motion used for the construction of modern numerical planetary ephemerides contains the equations for the Sun, the planets, the Moon, large asteroids, and TNOs. The masses of smaller bodies are poorly known, but they account for about 5 - 10% of the total mass of the main asteroid belt and $\sim 60\%$ of the mass of the Kuiper belt, and their gravitational attraction should be taken into account. Here we used two-dimensional discrete models to estimate the masses of the belts. The masses of both rings were determined by analyzing the motion of planets (dynamical method) from spacecraft radio data. The position of the Solar system barycenter during the calculations was controlled and remained unchanged.

In this paper we are interested in the masses of the main asteroid belt and the Kuiper belt in the context of a more adequate allowance for the gravitational influence of a large number of bodies concentrated in the belts on the motion of major planets. A proper allowance for the combined influence of numerous bodies in the belts is needed to construct a more accurate dynamical model of the Solar system and to obtain accurate planetary ephemerides. It is possible to properly determine the masses of the belts from their gravitational influence on the motion of primarily the planets closest to them. Highly accurate observational data on the positions of spacecraft in the vicinity of planets play a crucial role in refining the parameters of the belts. In particular, using Saturn's accurate observations obtained from Cassini radio observations is important for the Kuiper belt. To refine the masses of the belts, we used

updated databases for the main belt and TNOs, the observations of planets and spacecraft, and the new EPM2017 version of the IAA RAS planetary ephemerides.

EPM2017 PLANETARY EPHEMERIDES

The mass estimates for the Kuiper belt in this paper are based on the processing of observations for the latest version of the IAARAS EPM (Ephemerides of Planets and the Moon) ephemerides, EPM2017. The EPM2017 ephemerides contain the barycentric coordinates and velocities of the Sun, the eight planets, the dwarf planet Pluto, the three largest asteroids (Ceres, Pallas, Vesta), and four TNOs (Eris, Haumea, Makemake, Sedna) as well as the lunar libration parameters and the TT–TDB time scale difference. The ephemerides span a time interval of more than 400 years (1787–2214). In the EPM ephemerides the equations of motion for the Sun, the Moon, and the planets obey the relativistic Einstein–Infeld–Hoffmann equations in the inertial barycentric frame and the TDB time scale (Pitjeva and Pitjev 2014) with additional perturbations from the largest asteroids and TNOs, the asteroid and Kuiper rings, and the solar oblateness. The following bodies treated as material points were included in the dynamical system: the planets, the Moon, Pluto, the 301 largest asteroids, and the 30 largest TNOs. The Newtonian gravitational accelerations are assumed to be negligible in the case where both interacting bodies are neither the Sun, nor a planet, nor one of the following bodies: the Moon, Pluto, Ceres, Pallas, Vesta, Iris, and Bamberg. In other words, for 16 main objects the equations of motion include all of the mutual perturbations, while for the remaining asteroids and TNOs only the Newtonian mutual perturbations between them and the planets, the Moon, and the Sun are calculated.

The major modifications compared to the previous EPM versions concern the following:

- The new revised version of the software package ERA-8 (Pavlov and Skripnichenko 2015) using the C and Racket programming languages, the SQLite database, and the SOFA (Standards Of Fundamental Astronomy) library of astronomical calculations is employed.
- A new model of the Moon is orbital and rotational motion (Pavlov et al. 2016) based on the equations of lunar motion of the JPL DE430 ephemerides (Folkner et al. 2014) and recommended by geophysical and geodynamic models was constructed. The change in the gravitational potential of the Moon as a result of tidal and rotational deformations, the torque of the Moon’s liquid core, and the dissipation of energy under core friction against the crust are taken into account in the realization.
- The model for the motion of planets and other objects in the Solar system in which the models of solar motion and the barycenter equations were refined was updated. Two-dimensional discrete rotating rings of the main asteroid belt and the Kuiper belt were added to the dynamical model of the Solar system and 30 TNOs were included in the joint integration.

- The additional relativistic Lense – Thirring accelerations dependent on the solar rotation were included in the general model of motions of Solar system bodies (<http://iaaras.ru/en/dept/ephemeris/epm/2017/>).
- The number of observations increased – we used a total of ~ 800 thousand positional observations of planets and spacecraft (1913–2015) and lunar laser observations (LLOs) (1970–2016), including the new infrared LLOs and the Cassini and Messenger data.
- The data on a number of asteroids and TNOs were updated and refined, in particular, we used the new masses deduced in the Dawn spacecraft encounters with Vesta and Ceres as well as for binary asteroids or those and TNOs with satellites.

Refining the Model of Solar Motion and the Equations of the Solar System Barycenter

The equations of motion in the dynamical EPM model are specified in the Barycentric Celestial Reference System (BCRS) whose origin is at the Solar system barycenter. The relativistic barycenter of the point masses μ_i of bodies is defined as

$$\mathbf{b} = \frac{\sum_i \mu_i^* \mathbf{r}_i}{\sum_i \mu_i^*},$$

where \mathbf{r}_i is the position of body i and μ_i^* is its relativistic gravitational parameter:

$$\mu_i^* = \mu_i \left(1 + \frac{1}{2c^2} \dot{r}_i^2 - \frac{1}{2c^2} \sum_{j \neq i} \frac{\mu_j}{r_{ij}} \right)$$

The notation:

$\mu_i = Gm_i$, where G the gravitational constant, m_i is the mass of body i ; for the planets, except the Earth, and other objects the masses m_i also include the masses of their satellites;

c – the speed of light;

$r_{ij} = |r_{ij}| = |r_j - r_i|$.

The initial coordinates and velocities of all bodies in the dynamical system are shifted so that the conditions $\mathbf{b} = \mathbf{0}$ and $\dot{\mathbf{b}} = \mathbf{0}$ are fulfilled. This is achieved by solving the following system of equations by an iterative method:

$$\sum_i \mu_i^* \mathbf{r}_i = \mathbf{0},$$

$$\sum_i (\mu_i^* \mathbf{r}_i + \mu_i^* \dot{\mathbf{r}}_i) = \mathbf{0},$$

where $\dot{\mathbf{r}}_i$ is the velocity vector of body i .

An improvement realized in EPM2016 and subsequent ephemerides is the inclusion of the term $\dot{\mu}_i$ that was neglected in EPM2015 and earlier ephemerides.

The Sun is involved in calculating the accelerations, along with other bodies, with the mutual gravitational influence of the Sun, the planets, large asteroids, TNOs, and the introduced rings for modeling the total attraction from small bodies of the main asteroid belt and the Kuiper belt being taken into account.

A peculiarity of the BCRS is the uncertainty of its axes. The initial positions of the axes are close to the J2000 coordinate system. When the observations are processed, the rotation correction parameters ϵ_x , ϵ_y and ϵ_z are refined for the orientation of the final ephemerides in the International Celestial Reference Frame ICRF2 using special spacecraft observations on the background of quasars whose coordinates are given in ICRF2. The accuracy of the BCRS orientation in the ICRS is about 0.2 mas (Pitjeva et al. 2017).

The roundoff errors in the numerical integration lead to a slight drift of the Solar system barycenter in the model from the initial position at the coordinate origin. However, this drift is insignificant (in the interval from 1900 to 2020 it is less than 0.02 mm) and virtually negligible in problems of ephemeris astronomy.

Modeling the Gravitational Influence of the Main Asteroid Belt and the Kuiper Belt

When modern highly accurate planetary ephemerides are constructed, the system of equations that includes the equations of motion for the Sun, the Moon, the planets, and the 301 largest asteroids (with EPM1999) and largest TNOs (21 with with EPM2008 and 30 with EPM2015) is integrated. Such a direct inclusion in the general system of integration requires a thorough and careful refinement of the initial data and the masses of the asteroids and TNOs.

Dynamical mass estimates are available for a number of asteroids that spacecraft have approached, for asteroids and TNOs with satellites, and for large asteroids from their perturbations on Mars and the Earth determined by radar observations. Individual mass estimates for asteroids and TNOs can also be obtained from their density estimates by taking into account their diameters and taxonomic class, but with a considerably larger error up to $5 \cdot 10^{-12} M_{Sun}$. The total number of asteroids with estimated masses included in the EPM integration is 301 (Pitjeva and Pitjev 2016). For 46 asteroids the masses were inferred from individual perturbations. For 30 asteroids the masses were inferred from their perturbations of planets by processing the radar data from Martian spacecraft and landers. The masses of Eros, Vesta, and Ceres were estimated very accurately from the data of the NEAR and DAWN spacecraft that investigated these asteroids. For 13 asteroids with satellites different authors obtained quite accurate estimates of their masses. For the remaining 255 asteroids the masses were determined from their diameters and density estimates

for three taxonomic classes obtained when improving the EPM ephemerides. Thus, we found the total mass of 301 largest asteroids to be

$$M_{301aster} = (11.531 \pm 0.071) \times 10^{-10} M_{Sun} \quad (3\sigma).$$

The Pluto–Charon system was included in the model to construct the ephemerides from the first EPM versions. At the same time, this system also belongs to the Kuiper belt. Mass estimates are available for a number of Kuiper belt objects around which satellites were detected. For such 11 large objects (Table 1) the masses taken from various astronomical data sites were determined with a reasonably good accuracy.

Table 1. Mass estimates for large Kuiper belt objects with satellites

TNO	Mass, m_{\oplus}	TNO	Mass, m_{\oplus}
Eris	$(28.0 \pm 0.33) \times 10^{-4}$	Orcus	$(1.059 \pm 0.008) \times 10^{-4}$
Pluto+Charon	$(24.473 \pm 0.113) \times 10^{-4}$	2003 AZ ₈₄	$(0.69 \pm 0.33) \times 10^{-4}$
Haumea	$(6.71 \pm 0.067) \times 10^{-4}$	Salacia	$(0.73 \pm 0.03) \times 10^{-4}$
Makemake	$(4.35 \pm 0.84) \times 10^{-4}$	Varda	$(0.444 \pm 0.011) \times 10^{-4}$
2007 OR ₁₀	$(6.3 \pm 4.5) \times 10^{-4}$	2002 UX ₂₅	$0.209 \pm 0.005) \times 10^{-4}$
Quaoar	$(1.67 \pm 0.17) \times 10^{-4}$		

For the remaining 20 of the 31 largest TNOs the masses were estimated much more poorly; they were calculated from their diameters and densities. The total mass of the 31 individually estimated largest TNOs, including the Pluto–Charon system, is

$$M_{31TNO} = 0.0086 \pm 0.0017 m_{\oplus} \quad (3\sigma). \quad (1)$$

The masses of smaller bodies are poorly known, but they are variously estimated to be about 5-10% of the total mass of the main asteroid belt and 60% of the mass of the Kuiper belt. Their combined gravitational pull on the planets was also taken into account using a special model.

Allowance for the total additional attraction from the asteroids neglected individually in the joint numerical integration was first proposed by G.A. Krasinsky. The attraction from these objects was modeled by the attraction from a material circular ring located in the plane of the ecliptic with a uniform distribution of matter. The formulas for the disturbing force of the asteroid ring are given in Krasinsky et al. (2002). The mass of the ring M_r and its radius R_r were included in the set of parameters being improved. This model of a homogeneous ring was used in constructing the EPM2004 ephemerides (Pitjeva 2005). However, on the one hand, the asteroid belt is quite wide (more than 1 AU) and, on the other hand, there is a strong correlation between two parameters of the ring, its mass M_r and radius R_r , that does not allow them to be estimated with a good accuracy. Therefore, when constructing the EPM2013 ephemerides (Pitjeva and Pitjev 2014), we decided to pass to modeling the small bodies of the main asteroid belt by a two-dimensional ring with its radii specifying the boundaries of the model ring within which the bulk of

the belt bodies are located and which correspond to the two main 1 : 2 and 1 : 4 orbital resonances with the motion of Jupiter.

The situation with the Kuiper belt is similar. First we modeled the attraction from small TNOs by a one-dimensional ring located in the plane of the ecliptic with a radius of 43 AU and its estimated mass (Pitjeva 2010a, 2010b). In 2017, when constructing EPM2016 (Pitjeva et al. 2017), we used a two-dimensional rings of TNOs with the radii attributable to the 2 : 3 and 1 : 2 orbital resonances with the motion of Neptune.

Finding the gravitational potential and its derivatives for a flat material two-dimensional homogeneous ring leads to expressions that include complete elliptic integrals of the first, second, and third kinds. The calculation can be reduced to calculating the values of the hypergeometric function of the corresponding parameters by first applying the Landen transformation. The expressions for the potential and accelerations of the two-dimensional ring via the hypergeometric functions of four arguments were given in Pitjeva and Pitjev (2014, 2016). The formulas for the accelerations differ for points on the inside (closer to the Sun) and the outside (farther from the Sun) with respect to the two-dimensional circular ring. In 2017 they were first used for the Kuiper belt (Pitjeva et al. 2017).

A Discrete Rotating Model for the Belts

The one- and two-dimensional models used in the previous EPM2004–EPM2016 versions of the ephemerides to find the total gravitational attraction from small bodies in the belts had a disadvantage. When the mutual attraction between the planet and the belt was taken into account, the introduced ring model should have shifted as a whole, which does not correspond to the actual interaction between the planet and moving bodies in the belts. To avoid this disadvantage, in this paper we used a discrete rotating model. Note that, as in previous papers, we modeled not the belt and the motion in it, but its gravitational influence on the planets. The discrete models are a system of material points with equal masses located in the plane of the ecliptic and moving in the same (prograde) direction as the planets. The material points in the model do not interact between themselves. The gravitational attraction occurs between each of them with the Sun and planets. In the model the material points were arranged at the initial time uniformly on three circular lines with initial velocities corresponding to circular motion.

For the main asteroid belt the extreme lines of the model correspond to the 2.06 and 3.27 au boundaries within which the bulk of the asteroids are located. Outside these boundaries the number of asteroids drops sharply. These distances correspond to the 1 : 2 and 1 : 4 orbital resonances with the mean motion of Jupiter. The bulk of the small asteroids, asteroid fragments, and dust of the main belt are located in the same zone, but the fraction of all of them in the mass of the main belt is small, $\sim 5\text{--}10\%$. Sixty material points

were located on each of the extreme lines and the middle line with a radius of 2.67 au in the model.

For the Kuiper belt the extreme lines with the system of material points corresponded to the boundaries of the densest, “main” part (De Sanctis et al. 2001) of the belt ($R_1 = 39.4$ au and $R_2 = 48.7$ au). These distances correspond to the 2 : 3 and 1 : 2 orbital resonances with the mean motion of Neptune. Forty points were located on each of these lines. The third line $R_m = 44$ au corresponded to the observed crowding of objects near 44 au, the belt “kernel” (Petit et al. 2001; Bannister et al. 2016), and the number of model points on it was 80, twice as large as that on the extreme lines.

The total masses of each model were the parameters that were determined by processing the observational data.

Observational Data

The number of highly accurate observations on which the next EPM versions are based increases steadily, and the total number of observations used in the current EPM2017 version of the planetary ephemerides is more than 800 thousands. In this case, not the individual spacecraft measurements themselves, but the normal points into which the observations on one spacecraft revolution were combined are used, because these observations are correlated between themselves. However, the observations of Martian landers were not combined into normal points, because they were also used to study the rotation of Mars in addition to the determination of other parameters.

Table 2. The observations used to improve EPM2017 and to estimate the parameters, EPM2017

Planet	Radio observations		Optical observations	
	interval of observations	number of norm. points	interval of observations	number of observations
Mercury	1964–2015	1556	—	—
Venus	1961–2013	3621	—	—
Mars	1965–2014	46441	—	—
Jupiter + 4 sat.	1973–1997	51	1914–2013	14866
Saturn + 7 sat.	1979–2014	171	1913–2013	16455
Uranus + 4 sat.	1986	3	1914–2013	12550
Neptune + 1 sat.	1989	3	1913–2013	12404
Pluto	—	—	1914–2013	16674
Total	1961–2015	51846	1913–2013	72049

Table 2 gives the number of normal points for radar data and the number of observations for optical data. Only highly accurate radio measurements that span a time interval of more than half a century are currently used in constructing the ephemerides of the inner planets. The optical observations are several orders of magnitude less accurate and were not used for these planets.

The techniques for determining the parameters of planetary ephemerides by processing measurements of various types, from classical meridian obser-

vations of planets and their satellites to modern radio observations of planets and spacecraft, are described in Pitjeva (2005, 2013). In this paper we used the optical observations from 1913 up until all the accessible modern 2015 observations. The accuracies of modern optical CCD observations reach a few hundredths of an arcsecond; spacecraft trajectory observations are much more accurate: 1–2 m for the inner planets and about 20 m for the Cassini spacecraft (Hees et al. 2014). The optical observations with an acceptable accuracy span an interval slightly longer than one revolution for Uranus and slightly more than half of the complete revolution around the Sun for Neptune. From the radio measurements for Uranus and Neptune there is only one 3D point for each of the planets obtained during the Voyager-2 flyby. Most of the observations were taken from the database of the NASA Jet Propulsion Laboratory (JPL) created by M. Standish and being continued and maintained at present by W. Folkner: https://ssd.jpl.nasa.gov/?eph_data. These data were supplemented by the Russian radar observations of planets (1961–1995): <http://iaaras.ru/en/dept/ephemeris/observations/>, the Pulkovo Observatory optical data and the revised Lowell Observatory data (Buie and Folkner 2015), the new CCD data of the Brazilian Pico dos Dias Observatory (Benedetti-Rossi et al. 2014), and the Venus Express (VEX) and Mars Express (MEX) data retrieved by courtesy of A. Fienga,

<http://www.geoazur.fr/astrogeo/?href=observations/base>.

After the processing of all observations and the refinement of the EPM2017 parameters, Figs. 1–7 present the residuals of the ranging from the Earth to the planet for the observations of the Messenger, VEX, Mars Global Surveyor (MGS), Odyssey, MEX, Mars Reconnaissance Orbiter (MRO), and Cassini spacecraft revolving about Mercury, Venus, Mars, and Saturn.

It should be noted that for the observations near conjunctions of the planet with the Sun the scatter of residual increases significantly due to the influence of the solar corona (despite its reduction in the observations); therefore, these observations were removed. The root-mean-square (rms) deviations of the residuals (σ) of the method, wrms, for the corresponding sets of observations are given in the captions to the figures. The rms deviations are 0.7 m for the new Messenger observations, about 1 m for the Martian spacecraft, and 21.2 m for the Cassini spacecraft near Saturn. For the VEX spacecraft near Venus (2010–2012) the spacecraft orbit after 2010 passed near the upper layers of its atmosphere, occasionally touching it. Therefore, the scatter of residuals for the VEX observations is slightly larger than that for the Martian spacecraft, being about 3 m. Despite the fact that the agreement of the Martian observations became more difficult, because the interval of observations of the Martian spacecraft increased compared to EPM2011 by 3–4 years, the rms deviations for the Martian MGS, Odyssey, and MRO spacecraft nevertheless decreased by 10–20% due to the refinement of the models of planetary motions. The graphs of the residuals of spacecraft observations and the amplitudes of their scatter are close to those for the JPL NASA DE 430 ephemerides (Folkner et al. 2014), while the characteristics in Fig. 1 for the Messenger spacecraft are similar to the graph from Park et al. (2017).

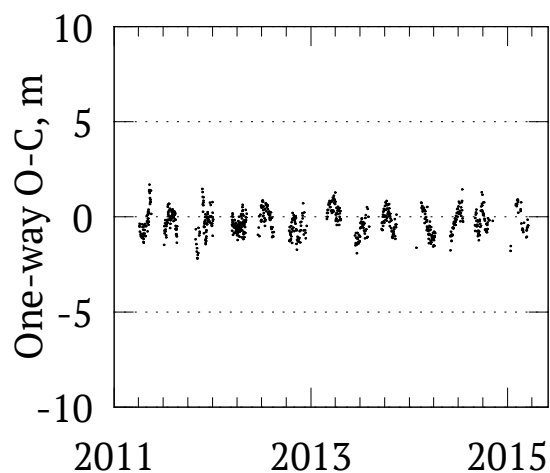


Fig. 1 O-C of the Messenger ranging (in one direction) calculated from the EPM2017 ephemerides, $\sigma = 0.7$ m.

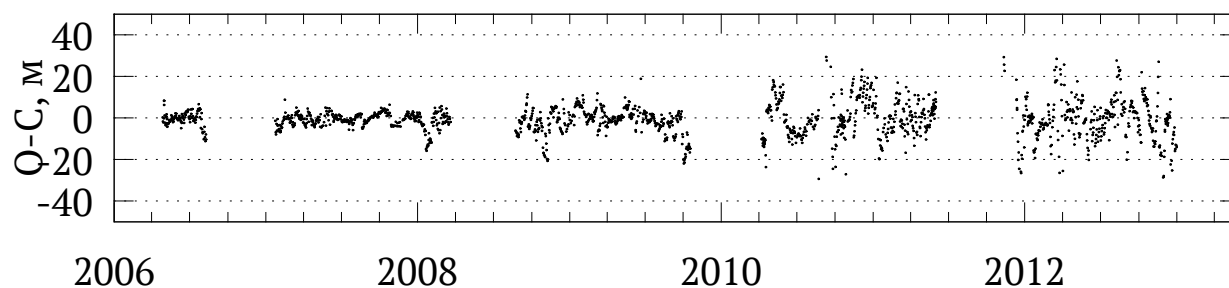


Fig. 2 O-C of VEX ranging (in one direction) calculated from the EPM2017 ephemerides, $\sigma = 2.98$ m.

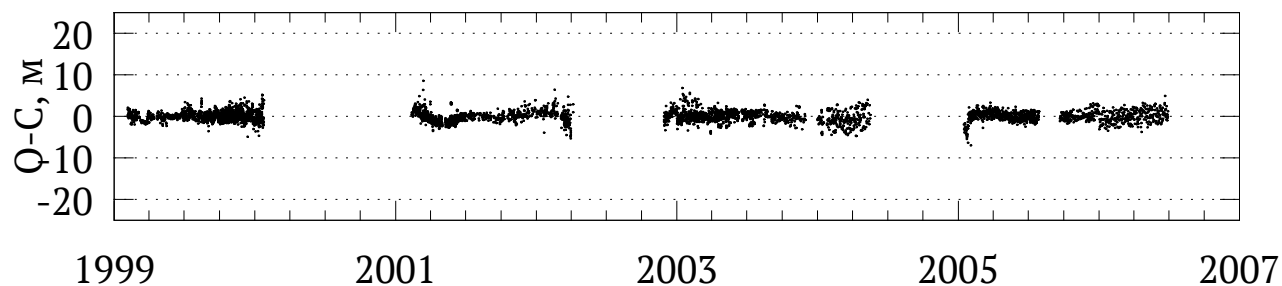


Fig. 3 O-C of MGS ranging (in one direction) calculated from the EPM2017 ephemerides, $\sigma = 1.17$ m.

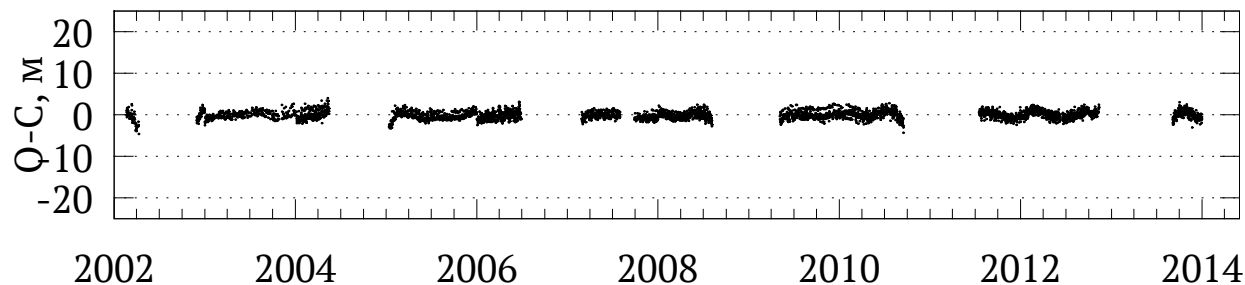


Fig. 4 O-C of Odyssey ranging (in one direction) calculated from the EPM2017 ephemerides, $\sigma = 0.95$ m.

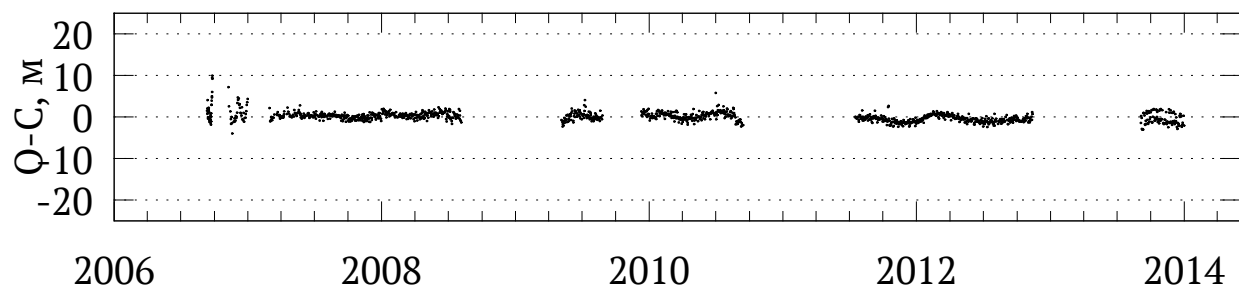


Fig. 5 O-C of the MRO ranging (in one direction) calculated from the EPM2017 ephemerides, $\sigma = 0.95$ m.

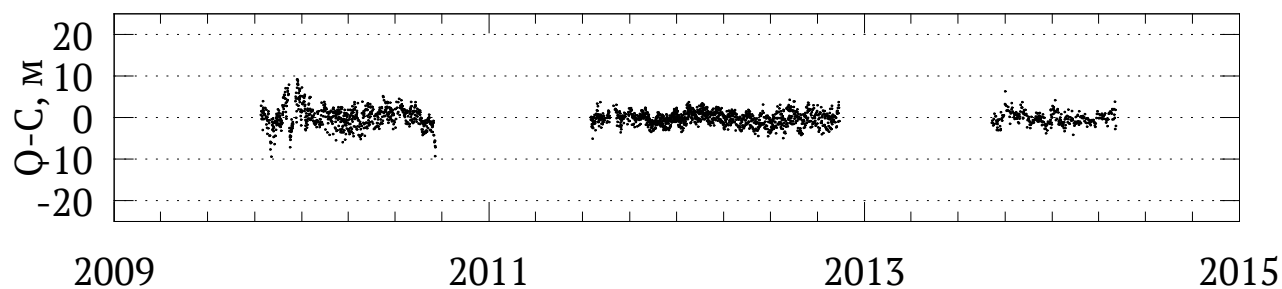


Fig. 6 O-C of the MEX ranging (in one direction) calculated from the EPM2017 ephemerides, $\sigma = 1.5$ m.

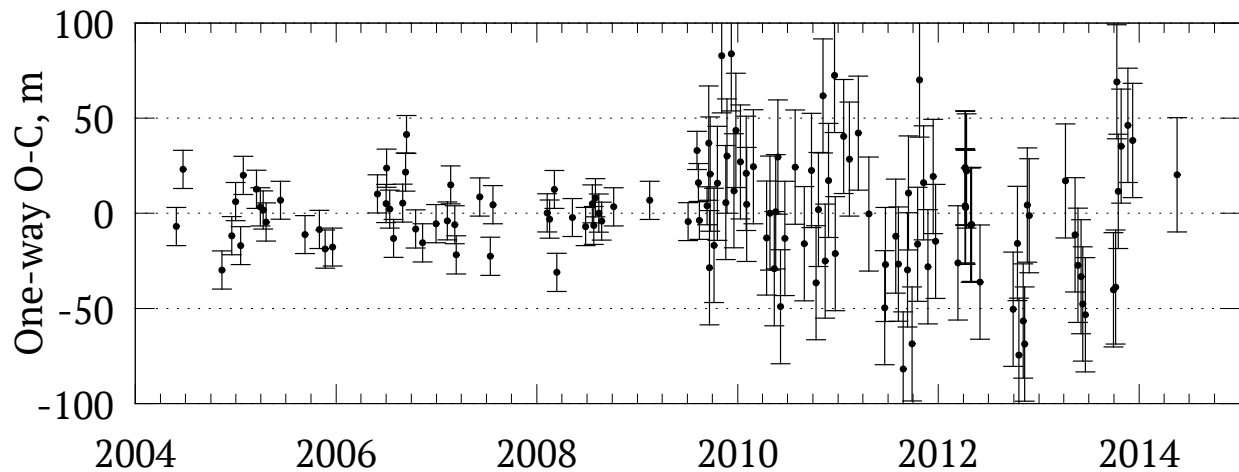


Fig. 7 O-C of the Cassini ranging (in one direction) calculated from the EPM2017 ephemerides, $\sigma = 20.2$ m.

Accuracies of the Orbital Elements of the EPM Ephemerides

Concurrently with the refinement of all parameters of the EPM2017 ephemerides, we also obtained their formal errors. Table 3 gives the formal standard errors of the orbital elements for the planets, where a is the semimajor axis, i is the orbital inclination, Ω is the longitude of the ascending node, e is the eccentricity, π is the longitude of perihelion, and λ is the mean longitude. The formal standard errors of the least squares method (LSM) for the semimajor axes of the inner planets are a few hundredths of a meter (Table 3), and although, as experience shows, the actual errors can be larger than the formal LSM errors by an order of magnitude, the accuracy of determining these and other orbital elements is high even if this is taken into account.

Table 3. Formal standard errors of the orbital elements for the planets calculated from the EPM2011 and EPM2017 ephemerides

Ephemerides	Planet	a [m]	$\sin i \cos \Omega$ [mas]	$\sin i \sin \Omega$ [mas]	$e \cos \pi$ [mas]	$e \sin \pi$ [mas]	λ [mas]
EPM2011	Mercury	0.170	0.8275	0.5639	0.0907	0.06885	0.1617
EPM2017	Mercury	0.0015	0.00152	0.00144	0.00084	0.00024	0.00337
EPM2011	Venus	0.089	0.00364	0.00288	0.00033	0.00020	0.00325
EPM2017	Venus	0.0065	0.00358	0.00349	0.00014	0.00016	0.00268
EPM2011	Earth	0.131	—	—	0.00043	0.00017	—
EPM2017	Earth	0.013	—	—	0.00008	0.0006	—
EPM2011	Mars	0.616	0.00143	0.00115	0.00142	0.00071	0.00278
EPM2017	Mars	0.0487	0.00084	0.00093	0.00008	0.00018	0.00037
EPM2011	Jupiter	351	2.008	1.811	0.129	0.110	0.884
EPM2017	Jupiter	372	1.749	1.629	0.163	0.133	1.070
EPM2011	Saturn	70.519	0.10792	0.12023	0.01093	0.00327	0.03434
EPM2017	Saturn	16.936	0.08176	0.05845	0.00368	0.00237	0.01732
EPM2011	Uranus	30075	3.458	4.013	2.853	2.006	3.598
EPM2017	Uranus	31314	3.574	3.806	2.716	2.238	2.833
EPM2011	Neptune	270853	2.673	5.202	5.554	13.558	12.363
EPM2017	Neptune	288035	3.769	5.381	5.791	14.386	12.536
EPM2011	Pluto	2022765	2.759	10.021	43.896	31.381	18.215
EPM2017	Pluto	790006	0.758	3.657	17.671	12.473	6.022

In addition, Table 3 shows, for comparison, the formal standard errors of the orbital elements for the planets calculated from the EPM2011 ephemerides. It should be noted that these standard errors were calculated for the EPM2011 and EPM2017 ephemerides using two different software packages, ERA-7 and ERA-8. Therefore, these errors slightly differ even when using the same observations. This can be seen using Neptune as an example, for which no new observations have been available since 2011. For Mercury the orbital elements became much more accurate, while their formal errors decreased by one or two orders of magnitude after the appearance of Messenger observations. The

formal errors of the orbital elements for Mars and the Earth decreased noticeably (occasionally by an order of magnitude) due to the large amount of new Odyssey, MRO, and MEX data. For Pluto the decrease in the errors of the orbital elements by several times is explained by the appearance of new highly accurate CCD observations obtained at the Pico dos Dias Observatory from 1995 to 2013 and revised Lowell Observatory data (1913–1951). For Venus the VEX mission ended in 2012 and no new observations have appeared, just as for Jupiter and Uranus; therefore, their errors barely changed. As yet no new observations from the Juno spacecraft near Jupiter are accessible.

The progress of EPM2017 in increasing the accuracy of planetary ephemerides is explained primarily by the use of new highly accurate trajectory data for various spacecraft as well as by an improvement in modeling the motions of planets and an improvement of the dynamical model.

MASS OF THE MAIN ASTEROID BELT

A large set of small bodies moving in nearly circular orbits between Mars and Jupiter, $1.8 \text{ au} < r < 3.5 \text{ au}$, belong to the main asteroid belt. The densest part of the belt is located in the band between the 1 : 4 (2.06 au) and 1 : 2 (3.27 au) orbital resonances with Jupiter. It contains more than 90% of all the numbered asteroids. These distances may be deemed to be, respectively, the inner and outer boundaries of the bulk of the main belt, because the number of asteroids drops sharply outside them.

Statistical and Dynamical Mass Estimates for the Asteroid Belt

The first estimates of the total mass for the belt were made by statistical methods. The distributions in apparent magnitudes obtained from observations, albedo estimates, deduced and empirical size distribution functions, and estimates of the mean densities of objects were used. For the asteroids of the main belt the mean densities depended on the taxonomic class to which a given asteroid was attributed. Since the statistical estimates depend on several assumptions and ill-defined parameters, the authors provide no errors of the statistical mass estimates (Table 4).

The mass of the belt was grossly overestimated in 1990 (McBride and Hughes 1990). Subsequently, the values of the mass were reduced. The latest paper on a statistical mass estimate was published in 2012 (Vinogradova 2012). Dynamical mass estimates for the main belt are obtained from its gravitational influence on the motion of other bodies in the Solar system, primarily on Mars nearest to the belt. Mass estimates for 301 large asteroids are presented in the Section “Modeling the Gravitational Influence of the Main Asteroid Belt and the Kuiper Belt”.

The total mass of the remaining small asteroids, asteroid fragments, and dust in the main belt was found in the EPM ephemerides from observations

Table 4. Statistical estimates of the total mass for the main asteroid belt

Year	Authors	Mass (in M_{\odot})
1990	McBride and Hughes	$\sim 55 \cdot 10^{-10}$
2001	Petit et al.	$15 \cdot 10^{-10}$
2012	Vinogradova	$13.5 \cdot 10^{-10}$

Table 5. Dynamical estimates of the total mass for the main asteroid belt

Year	Authors	Ephemerides	Mass (in M_{\odot})
2002	Krasinsky et al.	EPM2000	$(18 \pm 2) \cdot 10^{-10}$
2005	Pitjeva	EPM2004	$(15 \pm 1) \cdot 10^{-10}$
2013	Kuchynka and Folkner	DE 430	$(13.3 \pm 0.2) \cdot 10^{-10}$
2013	Pitjeva	EPM2011	$(12.3 \pm 1.2) \cdot 10^{-10}$
2014	Pitjeva and Pitjev	EPM2013	$(12.2 \pm 0.2) \cdot 10^{-10}$
2017	Pitjeva et al.	EPM2016	$(12.245 \pm 0.187) \cdot 10^{-10}$
2018	Pitjeva and Pitjev	EPM2017	$(12.038 \pm 0.0874) \cdot 10^{-10}$

using initially a one-dimensional ring with its estimated radius and mass (EPM2000–EPM2011) and subsequently using a two-dimensional ring with its radii determined by the 2.06 and 3.27 au resonances with the motion of Jupiter and the estimated mass (beginning with EPM2013).

The total mass of the main asteroid belt was found as the sum of the masses of the 301 largest asteroids and the estimated mass of the modeled asteroid ring. Table 5 gives previous mass estimates for the main asteroid belt. For comparison, the mass estimate for the asteroid belt obtained for the DE 430 ephemerides (Kuchynka and Folkner 2013) was also included in the table. In its paper the mass of the asteroid belt was found from the masses of 3714 asteroids estimated in two ways. For the largest 343 asteroids the masses were determined using Tikhonov’s regularization from the ranging measurements of Martian spacecraft and landers; for the remaining 3371 asteroids the mass estimates were obtained from their diameters deduced from infrared observations and the presumed mean density $\rho = 2.2 \text{ g cm}^{-3}$. The derived total mass of the belt in their paper is $13.3 \cdot 10^{-10} M_{\odot}$, with 90% of this mass being accounted for by 343 large asteroids.

In our paper to estimate the mass of the remaining, smaller asteroids, we used a discrete rotating model with radii $R_1 = 2.08 \text{ au}$ and $R_2 = 3.27 \text{ au}$ for the extreme lines and the middle line with radius $R_m = 2.66 \text{ au}$ and 60 material points on each of the lines and a total number of moving material points of 180 (see Section “A Discrete Rotating Model for the Belts”).

The total mass of the small asteroids, small fragments, and dust of the main belt was found from the discrete model to be

$$M_{discr.ring} = (0.507 \pm 0.051) \cdot 10^{-10} M_{sun} = (0.169 \pm 0.017) \cdot 10^{-4} m_{\oplus} (3\sigma).$$

The total mass of the main belt (in the sum with the mass of 301 large asteroids) is

$$M_{Main} = (12.038 \pm 0.087) \cdot 10^{-10} M_{sun} = (4.008 \pm 0.029) \cdot 10^{-4} m_{\oplus} (3\sigma).$$

The same mass is shown in the last row of Table 5. All of the mass estimates in this paper are given with an uncertainty equal to the 3σ standard error of the LSM. The mass of the small bodies and dust is about 4.5% of the total mass of the main belt. It can be seen from Table 5 that the error in estimating the total mass of the main asteroid belt decreases in each new EPM version due to an increase in the amount of observational data and an improvement of the models used for the mass estimates of the remaining small asteroids. The mass estimation accuracy improved approximately by a factor of 6 as we passed from the one-dimensional ring to the two-dimensional one and became better for the discrete rotating ring by a factor of 2. The representation of observations also improved. The residuals in processing the observations of the spacecraft near Venus and Mars are given in Figs. 1–6.

MASS OF THE KUIPER BELT

The Kuiper belt objects (KBOs) are divided (Jewitt et al. 1998; Gladman 2002), given the characteristics of their orbits, into three main dynamical classes: classical, resonant, and scattered disk objects.

Classical KBOs have nearly circular orbits and relatively small eccentricities. Their nearly circular orbits lies in the region 40–50 au from the Sun. These objects undergo no strong influence of the major planets; their orbits remain essentially unchanged. They are most numerous and constitute the bulk of the population. The plane of the Kuiper belt determined from classical objects with inclinations $|i| < 5^\circ$ agrees with the invariant plane of the Solar system (Elliot et al. 2005). The main classical Kuiper belt is located between the 3 : 2 and 2 : 1 orbital resonances with Neptune in the ring belt $39.4 \text{ au} < a < 47.8 \text{ au}$ (De Sanctis et al. 2001). There is a sharp outer edge in the distribution, the so-called Kuiper Cliff, a sharp drop in the number of classical objects after 50 au. To be more precise, beyond 48 au the number of objects with sizes larger than 40 km drops sharply (Jewitt et al. 1998; Trujillo and Brown 2001; Gladman et al. 2001; Allen et al. 2002). The outer boundary for the belt of classical objects is well-defined, and it may correspond to the edge of the primordial protoplanetary cloud.

There is a crowding in the distribution (“kernel”) with a concentration of orbits with semimajor axes $a \sim 44 \text{ au}$, eccentricities $e \sim 0.05$, and inclinations $|i| < 5^\circ$ (Petit et al. 2001; Bannister et al. 2016).

Primarily the objects in the 3 : 2 (plutino, $a \sim 39.4 \text{ au}$) and 2 : 1 ($a \sim 47.8 \text{ au}$) orbital resonances with the mean motion of Neptune are attributed to **resonant KBOs**, although there are some number of bodies with different resonance ratios of the mean motions.

Scattered disk objects (“wanderers”), objects with large eccentricities and large inclinations, with orbits extending far beyond 50 au (up to $a \sim 90 \text{ au}$ and $e \sim 0.5 - 0.6$ or larger) constitute the sparsest part.

The formation of such a belt structure is explained by perturbations from the planets and primarily from Neptune (Levison and Morbidelli 2003).

Statistical Mass Estimates for the Kuiper Belt

The first mass estimates for the Kuiper belt were obtained by statistical methods, where the parameters of the size distribution of bodies are used, which, in turn, are found from the distribution in apparent magnitudes. Because of the large distance to Kuiper belt objects, small objects are invisible even through large telescopes, and the size distribution function has to be extrapolated into the range of small diameters and the uncertainty of the result increases. Estimates of the mean density are also used. As a rule, the mean density is taken to be $1.5\text{--}2.0\text{ g cm}^{-3}$, because the Kuiper belt objects are icy bodies that incorporate frozen methane, ammonia, water, and carbon dioxide surrounding the rocky interiors. Generally, the statistical estimates have a large scatter and are based on various, not quite reliable assumptions about the albedo and density of belt objects. Because of their large uncertainties, the authors publish the mass estimates without providing any errors. Table 6 gives the values obtained by different authors. The scatter of estimates is large; the estimates lie within the range from $0.01 m_{\oplus}$ to $0.2 m_{\oplus}$.

In the suggested models of the formation of the Solar system a significant initial mass of the belt, $\sim 10 - 30m_{\oplus}$, is required for the formation of the Kuiper belt (Stern and Colwell 1997; Delsanti and Jewitt 2006; Kenyon 2002). The statistical mass estimates (Table 6) to date give a value that is smaller by two or three orders of magnitude. Therefore, various processes for strong and fast dispersal of the original cloud are suggested.

Table 6. Statistical mass estimates for the Kuiper belt

Year	Author	Mass	Note
1997	Weissman and Levison	$0.1 \div 0.3 m_{\oplus}$	Between 30 au and 50 au
1998	Jewitt et al.	$\sim 0.1 m_{\oplus}$	
1999	Chiang and Brown	$\sim 0.2 m_{\oplus}$	Between 30 au and 50 au
1999	Kenyon and Luu	$\sim 0.1 m_{\oplus}$	Between 30 au and 50 au
2001	Gladman et al.	$0.04 \div 0.1 m_{\oplus}$	Between 30 au and 50 au
2002	Luu and Jewitt	$0.01 \div 0.1 m_{\oplus}$	Between 35 au and 150 au
2002	Kenyon	$0.1 - 0.2 m_{\oplus}$	Total mass beyond the orbit Neptune
2004	Bernstein et al.	$0.010 m_{\oplus}$	Classic Kuiper belt
2009	Booth et al.	$0.03 m_{\oplus}$	Class. + scattered Kuiper belt
		$0.01 m_{\oplus}$	Classic objects
		$0.02 m_{\oplus}$	Scattered Kuiper objects
2010	Vitense et al.	$0.05 m_{\oplus}$	Classic + resonant objects
		$0.07 m_{\oplus}$	Scattered objects

Dynamical Mass Estimates for the Kuiper Belt

The Kuiper belt occupies a large volume of space and includes not only a great number of large objects, but also hundreds of thousands of smaller bodies. At the current accuracy of planetary ephemerides the attraction from the belt leads to a noticeable gravitational influence on the motion of bodies in the Solar system that should be properly taken into account.

The first dynamical mass estimates for TNOs in the Kuiper belt were made in 2010 (Pitjeva 2010a, 2010b) based on the EPM2008 ephemerides. In this case, the gravitational influence of a set of small or as yet undetected belt bodies was modeled by a one-dimensional material ring with a radius of 43 au in the plane of the ecliptic. The next mass estimates for the Kuiper belt were made in a similar way using the EPM2011 (Pitjeva 2013) and EPM2013 (Pitjeva and Pitjev 2014) ephemerides. The results are presented in Table 8. The data for the motion of Saturn obtained from Cassini radio measurements played an important role in the dynamical estimates found.

Table 8. Dynamical mass estimates for the Kuiper belt

Ephemerides	Mass of 1D/2D ring	Total mass of belt	References
EPM2008	$1.66 \cdot 10^{-2} m_{\oplus}$	$2.58 \cdot 10^{-2} m_{\oplus}$	Pitjeva(2010a, 2010b)
EPM2011	$(1.67 \pm 0.83) \cdot 10^{-2} m_{\oplus}$	$2.63 \cdot 10^{-2} m_{\oplus}$	Pitjeva(2013)
EPM2013	$(1.08 \pm 0.59) \cdot 10^{-2} m_{\oplus}$	$1.97 \cdot 10^{-2} m_{\oplus}$	Pitjeva and Pitjev(2014)
EPM2016	$(1.44 \pm 0.41) \cdot 10^{-2} m_{\oplus}$	$(2.28 \pm 0.46) \cdot 10^{-2} m_{\oplus}$	Pitjeva et al.(2017)
EPM2017	$(1.11 \pm 0.25) \cdot 10^{-2} m_{\oplus}$	$(1.97 \pm 0.30) \cdot 10^{-2} m_{\oplus}$	This paper

In EPM2016 (Pitjeva et al. 2017) we made a transition from modeling the total gravitational attraction from small belt objects using a one-dimensional ring (EPM2008–2015) to its modeling by a two-dimensional homogeneous ring. The densest part of the Kuiper belt is the ring zone between the two main 3 : 2 and 2 : 1 resonances with Neptune with the corresponding mean distances from the Sun ~ 39.4 and ~ 47.8 au. It contains the bulk of the Kuiper belt population and includes classical objects and the most numerous part of resonant belt objects. Since the number of objects outside this region drops significantly, the distances of 39.4 and 47.8 au were taken as, respectively, the inner and outer boundaries when modeling by the two-dimensional ring and when estimating the mass of the Kuiper belt. For Saturn there are quite accurate observational data that were obtained with the Cassini spacecraft and that are presently very important for refining the gravitational influence of the belt. The densest part of the belt occupies a wide ring region (the radial width exceeds 8 au), and modeling its gravitational influence by a two-dimensional ring makes it possible to more properly take into account the influence on the planets nearest to it whose orbits are comparatively close to the belt boundaries. It can be seen from our test calculations (Table 7) that the influence

of the two-dimensional ring differs noticeably from the influence of the one-dimensional ring with the same mass, especially on Uranus and Neptune.

Table 7. Shift of the perihelion of planets due to the influence of a homogeneous and two-dimensional ring over 100 years (in arcsec), $m = 2 \cdot 10^{-2} m_{\oplus}$

Planet	1 D	1 D	2 D
	R=43 au	R=44 au	$R_1 = 39.4$ au, $R_2 = 47.8$ au
Neptune	0''.0437	0''.0376	0''.0432
Uranus	0''.0095	0''.0086	0''.0091
Saturn	0''.0024	0''.0022	0''.0023
Jupiter	0''.0009	0''.0008	0''.0009
Mars	0''.0003	0''.0003	0''.0003

When using the two-dimensional ring as a model (EPM2016, Pitjeva et al. 2017), we obtained the following estimates:

the mass of the modeled TNO ring

$$M_{TNO\text{ring}} = (1.44 \pm 0.41) \cdot 10^{-2} m_{\oplus} (3\sigma),$$

and the total mass of the Kuiper belt

$$M_{Kuiper} = (2.28 \pm 0.46) \cdot 10^{-2} m_{\oplus} (3\sigma).$$

The dynamical masses determinations for the Kuiper belt are given in Table 8.

In this paper we obtained a new mass estimate for the Kuiper belt using a **discrete rotating model** for the attraction from small or as yet undetected belt bodies and small fragments (the Section ‘‘A Discrete Rotating Model for the Belts’’). Their combined gravitational influence was modeled with the model parameters $R_1 = 39.4$, $R_2 = 48.7$, $R_m = 44$ au and a total number of material points of 160: we took 40 points for each of the $R_1 = 39.4$ and $R_2 = 48.7$ lines; for the densest part of the belt with a mean radius $R_m = 44$ au we took 80 points.

The mass of the modeled part of the belt was found to be

$$M_{TNO\text{ring}} = (1.11 \pm 0.25) \cdot 10^{-2} m_{\oplus} (3\sigma). \quad (2)$$

Thus, the final result for **the total mass of the belt**, including all of the large (Eq. (1)) and small (Eq. (2)) bodies, turned out to be

$$M_{Kuiper} = (1.97 \pm 0.30) \cdot 10^{-2} m_{\oplus} (3\sigma). \quad (3)$$

This estimate is given in the last row of Table 8.

As yet there are no dynamical mass estimates for the Kuiper belt made by other authors.

CONCLUSIONS

We obtained new mass estimates for the main asteroid belt and the Kuiper belt based on the revised EPM2017 planetary ephemerides on the new ERA–8 software platform and the software part for the motion of the Moon. We used $\sim 800\,000$ positional observations of planets and spacecraft (1913–2015). To estimate the mass of the part of the belts that consists of numerous small or as yet undetected belt objects, we modeled the gravitational attraction using a discrete rotating system of material points. For the main asteroid belt the total mass was found to be

$$M_{belt} = (12.038 \pm 0.087) \cdot 10^{-10} M_{sun} = (4.008 \pm 0.029) \cdot 10^{-4} m_{\oplus} (3\sigma).$$

The total mass for the Kuiper belt is

$$M_{Kuiper} = (1.97 \pm 0.30) \cdot 10^{-2} m_{\oplus} \quad (3\sigma).$$

The error in estimating both the modeled part of the belts and the total mass of the asteroid and Kuiper belts decreased considerably from 2006 to 2017. This is due to an increase in the number of observations and an improvement of their quality as well as a refinement of the models for the belts. Applying the discrete model led to a better representation of the observations (Figs. 1–7) and a refinement of the orbital elements for the planets (Table 3).

ACKNOWLEDGMENTS

We thank D.A. Pavlov for the development of the ERA software package that allowed us to take an important step in developing the EPM ephemerides and the EPM2017 version: including the additional relativistic Lense–Thirring accelerations in the general model to integrate the differential equations; improving the determination of the Solar system barycenter; modeling the Sun's accelerations; integrating the isochronous derivatives. We are also grateful to M.A. Bodunova for her calculations of the influence of the model rings on the planets. This work was supported by the “Cosmos: Studies of Fundamental Processes and Their Interrelationships” Program no. 28 of the Presidium of the Russian Academy of Sciences.

References

1. R. L. Allen, G. M. Bernstein, and R. Malhotra, *Astron. J.* **124**, 2949 (2002).
2. M. T. Bannister, J. J. Kavelaars, J.-M. Petit, B. J. Gladman, S. D. J. Gwyn, Y.-T. Chen, K. Volk, M. Alexandersen, et al., *Astron. J.* **152**, 70 (2016).
3. G. Benedetti-Rossi, R. Vieira Martins, J. I. B. Camargo, M. Assafin, and F. Braga-Ribas, *Astron. Astrophys.* **570**, A86 (2014).
4. G. M. Bernstein, D. E. Trilling, R. L. Allen, M. E. Brown, M. Holman, and R. Malhotra, *Astron. J.* **128**, 1364 (2004).
5. M. Booth, M. C. Wyatt, and A. Morbidelli, *Mon. Not. R. Astron. Soc.* **399**, 385 (2009).
6. M. Buie and W. M. Folkner, *Astron. J.* **149**, 22 (2015).

7. E. I. Chiang and M. E. Brown, *Astron. J.* **118**, 1411 (1999).
8. A. Delsanti and D. Jewitt, in *Solar System Update*, Ed. P. Blondel and J. Mason (Springer, Berlin, 2006), p. 267.
9. J. L. Elliot, S. D.Kern, K. B.Clancy, A. A. S. Gulbis, R. L. Millis, M.W. Buie, L. H.Wasserman, E. I. Chiang, et al., *Astron. J.* **129**, 1117 (2005).
10. W. M. Folkner, J. G. Williams, D. H. Boggs, R. S. Park, and P. Kychynka, *IPN Prog. Rep.* **42-196** (2014).
11. B. Gladman, *Highlights Astron.* **12**, 193 (2002).
12. B. Gladman, J. J. Kavelaars, J.-M. Petit, A. Morbidelli, M. J. Holman, and T. Loredó, *Astron. J.* **122**, 1051 (2001).
13. A.Hees, W. Folkner, R. Jacobson, and R. Park, *Phys. Rev. D* **89**, 102002 (2014).
14. D. Jewitt, J. Luu, and C. Trujillo, *Astron. J.* **115**, 2125 (1998).
15. S. Kenyon, *Publ. Astron. Soc. Pacif.* **114**, 265 (2002).
16. S. J. Kenyon and J. Luu, *Astron. J.* **118**, 1101 (1999).
17. G. A. Krasinsky, E. V. Pitjeva, M. V. Vasilyev, and E. I. Yagudina, *Icarus* **158**, 98 (2002).
18. P. Kuchynka and W. Folkner, *Icarus* **222**, 243 (2013).
19. H. F. Levison and A. Morbidelli, *Nature (London, U.K.)* **426**, 419 (2003).
20. J. X. Luu and D. C. Jewitt, *Ann. Rev.* **40**, 63 (2002).
21. N. McBride and D.W. Hughes, *Mon. Not. R. Astron. Soc.* **244**, 513 (1990).
22. R. S. Park, W. M. Folkner, A. S. Konopliv, J. G. Williams, D. E. Smith, and M. T. Zuber, *Astron. J.* **153**, 121 (2017).
23. D. A. Pavlov and V. I. Skripnichenko, in *Proceedings Journées 2014 on Systemes de Reference Spatio-Temporels*, Ed. by Z. Malkin and N. Capitaine (Pulkovo Observ., 2015), p. 243.
24. D. A. Pavlov, J. G. Williams, and V. V. Suvorkin, *Celest.Mech. Dyn. Astron.* **126**, 61 (2016).
25. J.-M. Petit, A. Morbidelli, and J. Chambers, *Icarus* **153**, 338 (2001).
26. E. V. Pitjeva, N. P. Pitjev, D. A. Pavlov, and M. A. Bodunova, *Tr. IPA RAN* **43**, 113 (2017).
27. E. V. Pitjeva, *Solar Syst. Res.* **39**, 176 (2005).
28. E. V. Pitjeva, in *Proceedings of the IAU Symposium 263 on Icy Bodies of the Solar System*, Ed. by D. Lazzaro, D. Pralnik, R. Schulz, and J. A. Fernandez (Cambridge Univ. Press, Cambridge, 2010a), p. 93.
29. E. V. Pitjeva, in *Protecting the Earth against Collisions with Asteroids and Comet Nuclei*, Ed. by A. Finkelstein, W. Huebner, and V. Shor (Nauka, St. Petersburg, 2010b), p. 237.
30. E. V. Pitjeva, *Solar Syst. Res.* **47**, 386 (2013).
31. E. V. Pitjeva and N. H. Pitjev, *Celest. Mech. Dyn. Astron.* **119**, 237 (2014).
32. E. V. Pitjeva and N. H. Pitjev, in *Proceedings of the IAU Symp. No. 318 on Asteroids: New Observations, New Models*, Ed. by S. Chesley, A. Morbidelli, R. Jedicke, and D. Farnocchia (Cambridge Univ. Press, Cambridge, 2016), p. 212.
33. M. C. de Sanctis, M. T. Capria, and A. Coradini, *Astron. J.* **121**, 2792 (2001).
34. S. A. Stern and J. E. Colwell, *Astrophys. J.* **490**, 879 (1997).
35. C. A. Trujillo and M. E. Brown, *Astrophys. J.* **554**, L95 (2001).
36. T. Vinogradova, *Tr. IPA RAN* **26**, 110 (2012).
37. C. Vitense, A. Krivov, and T. Lohne, *Astron. Astrophys.* **520**, A32 (2010).
38. P. R. Weissman and H. F. Levison, Ed. by A. Stern and D. J. Tholen (Univer. Arizona Press, Tucson, 1997), p. 559.